tvst

https://doi.org/10.1167/tvst.8.4.16

Article

Performance of a Defect-Mapping Microperimetry Approach for Characterizing Progressive Changes in Deep Scotomas

Zhichao Wu[1,2], Roberta Cimetta[1,2], Emily Caruso[1,2], and Robyn H. Guymer[1,2]

[1] Centre for Eye Research Australia, Royal Victorian Eye and Ear Hospital, East Melbourne, Australia
[2] Ophthalmology, Department of Surgery, The University of Melbourne, Melbourne, Australia

Correspondence: Zhichao Wu, Centre for Eye Research Australia, Level 7, 32 Gisborne St, East Melbourne, VIC 3002, Australia. e-mail: wu.z@unimelb.edu.au

Received: 30 January 2019
Accepted: 18 June 2019
Published: 1 August 2019

Keywords: microperimetry; scotoma; progression; test–retest

Citation: Wu Z, Cimetta R, Caruso E, Guymer RH. Performance of a defect-mapping microperimetry approach for characterizing progressive changes in deep scotomas. Trans Vis Sci Tech. 2019;8(4):16, https://doi.org/10.1167/tvst.8.4.16

Purpose: To examine whether a microperimetry testing strategy based on quantifying the spatial extent of functional abnormalities (termed "defect-mapping" strategy) could improve the detection of progressive changes in deep scotomas compared to the conventional thresholding strategy.

Methods: A total of 30 healthy participants underwent two microperimetry examinations, each using the defect-mapping and thresholding strategies at the first visit to examine the test–retest variability of each method. Testing was performed using an isotropic stimulus pattern centered on the optic nerve head (ONH), which acted as a model of a deep scotoma. These tests were repeated at a second visit, except using a smaller stimulus pattern and thereby increasing the proportion of test locations falling within the ONH (to simulate the progressive enlargement of a deep scotoma). The extent of change detected between visits relative to measurement variability was compared between the two strategies.

Results: Relative to their effective dynamic ranges, the test–retest variability of the defect-mapping strategy (1.8%) was significantly lower compared to the thresholding strategy (3.3%; $P < 0.001$). The defect-mapping strategy also captured a significantly greater extent of change between visits relative to variability ($-4.70\ t^{-1}$) compared to the thresholding strategy ($2.74\ t^{-1}$; $P < 0.001$).

Conclusions: A defect-mapping microperimetry testing strategy shows promise for capturing the progressive enlargement of deep scotomas more effectively than the conventional thresholding strategy.

Translational Relevance: Microperimetry testing with the defect-mapping strategy could provide a more accurate clinical trial outcome measure for capturing progressive changes in deep scotomas in eyes with atrophic retinal diseases, warranting further investigations.

Introduction

A major challenge in the evaluation of new treatments for eyes with atrophic age-related macular degeneration (AMD) and inherited retinal diseases (IRDs) is the lack of clinical outcome measures that can accurately capture disease progression. As a result, large and lengthy clinical trials are often needed to be sufficiently powered to detect clinically meaningful treatment effects, especially given the often slowly progressive nature of these conditions. Therefore, better clinical outcome measures, especially functional outcome measures (which are preferred by regulatory authorities over anatomic outcome measures[1]), are urgently needed to improve the feasibility of evaluating new treatments for atrophic AMD and IRDs.

Fundus-tracked perimetry, typically referred to as "microperimetry," is a technique with the potential to address this need. With this technique, measurements of luminance increment sensitivity are obtained at specific retinal locations by using a scanning laser ophthalmoscope to visualize the retina throughout

the examination. Microperimetry has been used increasingly in recent years as an outcome measure in clinical trials,[2–14] or are being evaluated in observational studies in preparation for clinical trials,[15–19] for atrophic AMD and IRDs.

Conventionally, microperimetry testing involves using a thresholding strategy to obtain measurements of visual sensitivity through sampling each location multiple times with different stimulus intensities. With this approach, however, only a limited number of locations can be sampled when seeking to maintain reasonable test durations. Such an approach may suboptimally capture the progressive enlargement of atrophic or degenerative changes occurring in eyes with atrophic AMD and IRDs, and an approach based on quantifying the spatial extent of functional abnormalities may allow disease progression to be better characterized.

As such, we sought to determine whether a testing strategy that quantifies the spatial extent of functional abnormalities (which we termed a "defect-mapping" strategy) could allow progressive enlargement of deep scotomas to be better characterized than the conventional thresholding strategy. To examine this, we used the optic nerve head (ONH) of healthy participants as a model of a deep scotoma (in a similar manner as we had performed previously[20]) in a proof-of-principle study of this approach.

Methods

This study was approved by the human research ethics committee of the Royal Victorian Eye and Ear Hospital (RVEEH) and was conducted in adherence with the Declaration of Helsinki, with all participants providing written informed consent after an explanation of the study.

Participants

This study included healthy participants over 18 years old, and they were required to be free from any ocular or systemic conditions that could affect visual function (e.g., amblyopia or multiple sclerosis) or cognition (e.g., stroke); participants were allowed to have peripapillary atrophy, except if it was caused by ocular pathology (such as pathologic myopia). Participants who were taking any medication known to affect visual function (e.g., hydroxychloroquine), or who had any physical or mental impairment that prevented them from participating in this study or from providing informed consent were excluded from this study.

Microperimetry Testing

All microperimetry examinations were performed using the Macular Integrity Assessment (MAIA; CenterVue, Padova, Italy) device without pupillary dilation. Details about the device used in this study have been described previously,[20,21] but briefly: Goldmann Size III stimuli (0.43° in diameter) were presented for 200 ms against a background of 1.27 cd/m^2, with the maximum and minimum luminance of the stimuli that could be presented being 318 cd/m^2 and 1.35 cd/m^2, respectively (thus, providing a 36 dB dynamic range of differential contrast). Stimulus presentations at precise retinal locations were enabled by using a line-scanning laser ophthalmoscope with an infrared illumination system to track the fundus at 25 frames per second. Only one eye was examined in this study, and the study eye was selected at random.

In this study, two different test strategies for characterizing deep scotomas were evaluated: (1) a 4-2 staircase thresholding strategy and (2) a defect-mapping strategy, which involved single presentations of 10 dB stimuli at each location. Two tests for each testing strategy were performed during each visit (using the follow-up option to enable retesting at the same locations on the second test), alternating the strategy used for the four tests and randomizing which test strategy was performed first. These tests were performed again at a second visit using a smaller stimulus pattern to evaluate their performance at capturing simulated progressive changes in deep scotomas. During the first visit, an isotropic stimulus pattern consisting of 36 points that covered a 10° × 10° region (interstimulus spacing of 2°) centered on the ONH was used when evaluating the threshold strategy. A similar stimulus pattern consisting of 169 points covering the same region (interstimulus spacing of 0.83°) was used when evaluating the defect-mapping strategy, which provided a similar test duration to the tests performed using the threshold strategy. This was to ensure that the two testing strategies were compared equivalently, as the accuracy of the results are dependent on the amount of time spent on obtaining the measurements. On the second visit, the same stimulus patterns were used and also centered on the ONH (differences in positioning from the first visit would have a minimal impact given that the stimulus pattern covers the entire ONH), with the exception that the test locations covered a 9° × 9° region instead (interstimulus spacing of 1.8° and 0.75°

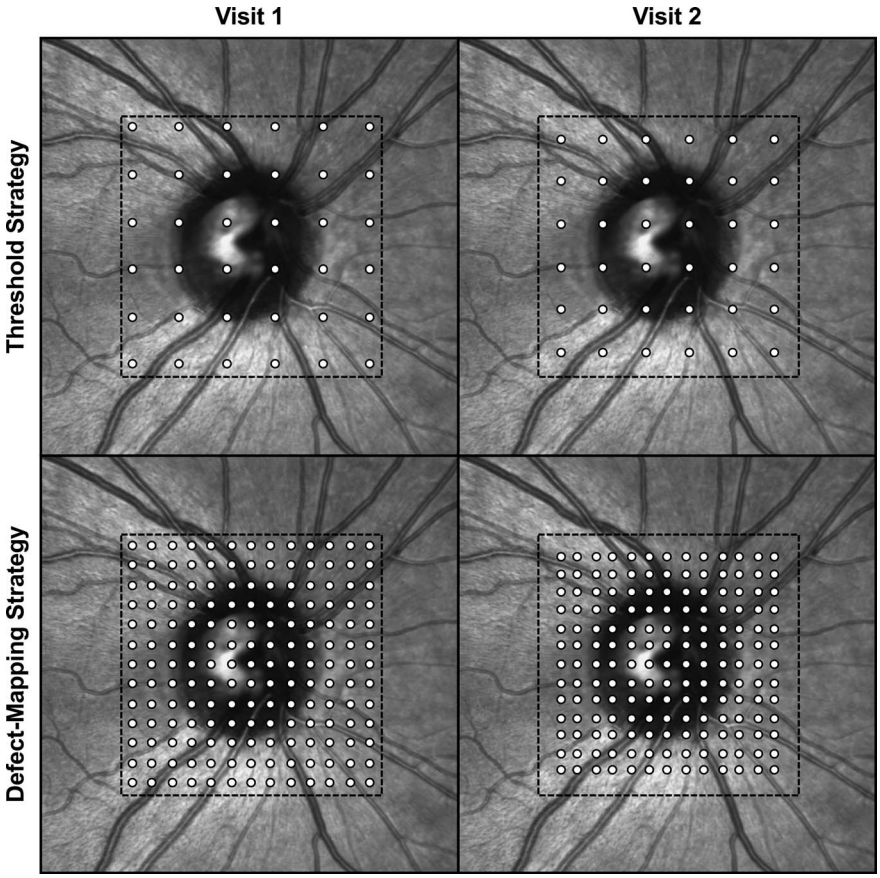

Figure 1. Stimulus patterns used for the microperimetry threshold and defect-mapping testing strategies on visits 1 and 2. *Dashed box* is shown to provide a reference to appreciate the difference in the size of the stimulus pattern between the two visits.

for the threshold and defect-mapping strategies, respectively). This modification increases the proportion of test locations that fell within the ONH, which simulates what might occur with the progressive enlargement of a deep scotoma. The stimulus patterns used are illustrated in Figure 1.

Identical verbal instructions then were given to all participants regarding how to perform in the microperimetry test, and a short practice test using the threshold strategy was performed if the participant had not previously performed perimetry testing. The reliability for each test was assessed by the frequency of false-positive responses to presentations of suprathreshold stimuli to the ONH, which was manually located on the microperimeter before presentation of the first stimuli; tests with false-positive responses of more than 25% were considered unreliable and were repeated.

Statistical Analysis

The mean sensitivity (MS; in decibels [dB]) was calculated for the microperimetry tests performed using the threshold strategy and proportion of locations seen (PLS; %) was calculated for the tests performed using the defect-mapping strategy.

The test–retest variability of MS and PLS was calculated relative to their effective dynamic range to enable equivalent comparisons between the two parameters as follows:

1. Effective Dynamic Range: The effective dynamic range of the thresholding strategy was defined as the average threshold of the edge points ($n = 20$) of the stimulus pattern from all tests of all participants at each visit, since these locations represent areas of normal function. Similarly, the effective dynamic range of the defect-mapping strategy was defined as the average PLS of the edge points ($n = 48$). The average sensitivity and PLS were determined using random-coefficients models, a form of linear mixed-effects model to account for within-eye correlations.
2. Test–Retest Variability: Based on probability theory, the standard deviation (SD) of test–

retest differences that follow a normal distribution with a mean of zero can be calculated by multiplying the mean absolute difference by $2/\sqrt{\pi}$. Thus, the SD was calculated using this method for each participant during each visit and then expressed as a percentage of the effective dynamic range (providing a normalized value of variability).
3. Comparison of Normalized Variability: The differences in the normalized SD between the two methods then were compared using another random-coefficients model.

The primary outcome measure in this study is the ability to detect change after accounting for measurement variability (to enable equivalent comparisons between the two testing strategies), evaluated using longitudinal signal-to-noise ratios (SNRs)[22–24] that were calculated as follows:

1. Variability of Each Method: This parameter was calculated by dividing the change in MS or PLS between visits by an estimate of its variability for each method. The estimates of variability were determined by first calculating best linear unbiased predictions for each eye using a linear mixed model (which are in essence predictions of the degree of change between the two visits, like a slope estimate). The SDs of the difference between the measured and predicted values then were calculated for each method to provide the estimate of variability.
2. Normalization of Change: The changes in MS and PLS between the two visits then were divided by their respective variability estimates to provide normalized estimates of change (or longitudinal SNRs); note that longitudinal SNRs are expressed as a ratio (which is a dimensionless quantity) per unit of time (t^{-1}).
3. Comparison of Normalized Estimates of Change: Another random-coefficients model was used to compare the normalized estimates of change (or longitudinal SNRs) between the two methods.

Results

Participant Characteristics

A total of 30 participants were included in this study, and their mean ± SD age was 36 ± 6 years (range, 25–53 years). Median time between the two visits was 2 weeks (interquartile range = 1–4 weeks).

Test–Retest Variability

The effective dynamic ranges of MS for the first and second visits were 25.7 and 25.1, dB respectively, and they were 98.6% and 98.3%, respectively, for the PLS. The SD of the effective dynamic range-adjusted test–retest variability of MS (3.3%) was significantly higher than the variability of PLS (1.8%; difference = −1.5%, 95% confidence interval [CI] = −2.0 to −0.7%; $P < 0.001$). Plots of the test–retest differences against the average of the two tests for the unadjusted values are shown in Figure 2 separately for each visit.

Three examples of the test–retest variability of the two testing strategies are shown in Figure 3, illustrating how the defect-mapping strategy allows a precise characterization of the spatial extent of the deep scotoma, while threshold-based measurements can be variable especially at the edge of the deep scotomas.

Detection of Change Over Time

There was a statistically significant change in MS (−1.5 dB, 95% CI = −1.9 to −1.0 dB; $P < 0.001$) and PLS (−5.4%, 95% CI = −6.3% to −4.4%; $P < 0.001$) between the two visits (being the estimates of "signal"). The standard deviations of the residuals (being an estimate of "noise") were 0.5 dB for MS and 1.1% for PLS. As such, the longitudinal SNR was significantly more negative (or a greater degree of change was detected relative to variability) for PLS ($-4.70\ t^{-1}$) compared to MS ($-2.74\ t^{-1}$; difference = $-1.96\ t^{-1}$, 95% CI = -2.93 to $-1.00\ t^{-1}$; $P < 0.001$). The best linear unbiased predictions of the normalized values of change are illustrated in Figure 4.

Two examples of changes over time simulated by decreasing the size of the stimulus pattern (or increasing the size of the deep scotoma) are shown in Figure 5. In both examples, expansion of the area of the deep scotoma relative to the stimulus pattern was generally poorly captured by the threshold strategy due to the large interstimulus spacing, while the defect-mapping strategy allowed the progressive changes to be better characterized.

Testing Duration and Reliability

The average test duration, beginning from capture of the reference fundus image to completion of the examination, was significantly shorter (–0.5 minutes, 95% CI = 0.4–0.6 minutes, $P < 0.001$) for the microperimetry tests using the defect-mapping strategy (5.3 minutes) compared to the threshold strategy (5.8 minutes). Furthermore, a total of seven (5.8%)

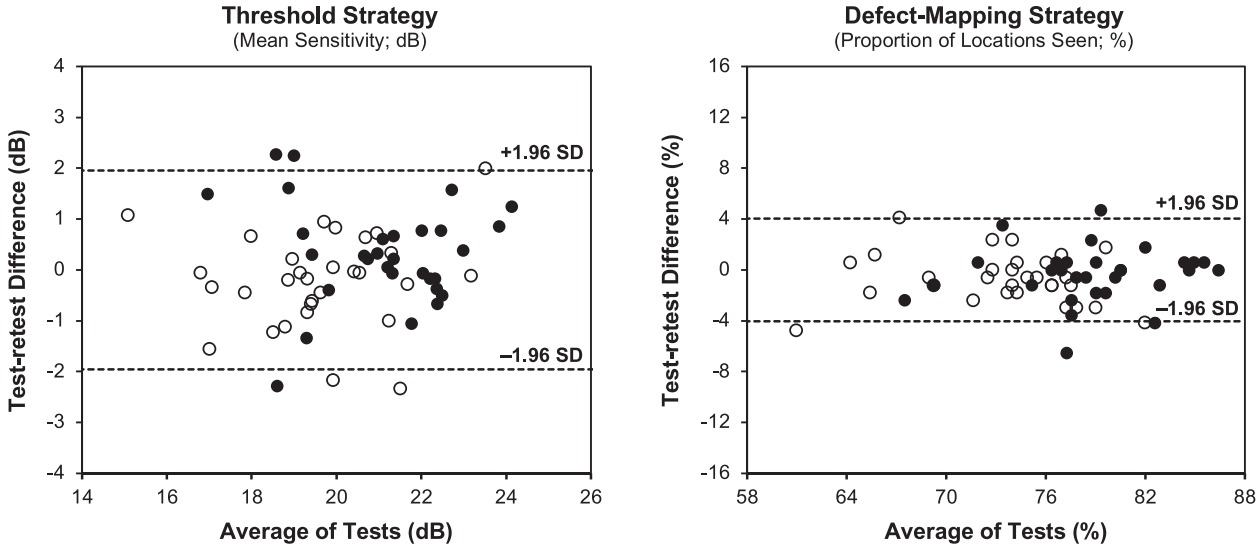

Figure 2. Bland-Altman plots of the test–retest difference of the threshold and defect-mapping microperimetry testing strategies plotted against the average value from the two tests shown for the first (*filled circles*) and second (*unfilled circles*) visits separately; *horizontal dashed lines* represent upper and lower 95% CIs (SD, standard deviation).

and three (2.5%) tests using the thresholding and defect-mapping strategy, respectively, had to be repeated due to poor reliability.

Discussion

This study revealed that a defect-mapping microperimetry testing strategy exhibited a nearly 2-fold reduction in test–retest variability compared to the conventional thresholding strategy. This also translated into a nearly 2-fold improvement in the ability to detect a simulated progressive enlargement of deep scotomas with the defect-mapping strategy. These findings highlight the potential value of the defect-mapping strategy and warrant further investigations to determine whether this approach could allow disease progression in eyes with atrophic AMD and IRDs to be more effectively characterized.

This is the first study to our knowledge that has equivalently compared an approach that quantifies

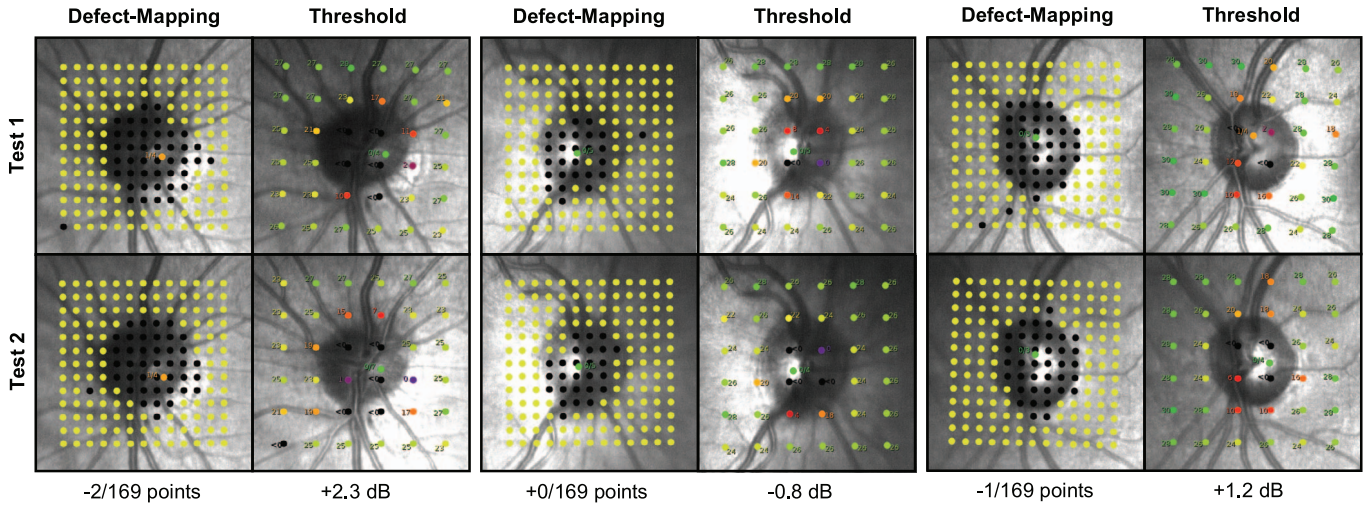

Figure 3. Examples of test–retest variability of the defect-mapping and threshold microperimetry testing strategies in this study from three different representative participants, with the outcome measures being the proportion of locations seen and mean sensitivity, respectively. Note that the additional test location that is not consistent with the isotropic stimulus pattern represents the location where the false-positive catch trials were presented.

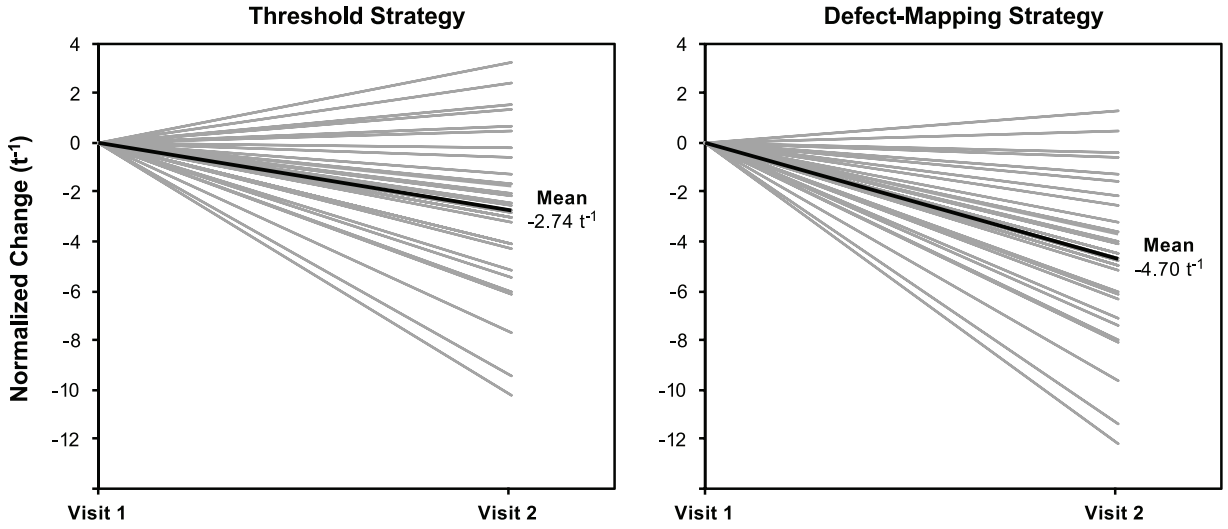

Figure 4. Normalized values of change over the two visits using the threshold and defect-mapping strategy on microperimetry, illustrating how the latter detected a greater degree of change relative to variability over the two visits.

the spatial extent of functional abnormalities to the conventional approach of measuring visual sensitivity thresholds. The superior performance of the defect-mapping strategy at capturing simulated progressive enlargement of deep scotomas when compared to a thresholding strategy may be attributed to several factors. First, we previously observed that test–retest variability at the border of deep scotomas was high when using a thresholding strategy,[20] meaning that this approach may have a limited ability to accurately measure the extent of functional abnormalities in eyes with deep scotomas. Second, the simulated progressive enlargement of deep scotomas may not be captured with the thresholding strategy due to the larger spacing between stimuli with this approach compared to the defect-mapping strategy. This may perhaps account for the recent observation of a nonsignificant treatment effect on the change in microperimetric threshold sensitivities in a recent trial of eyes with macular telangiectasia type 2, despite a significant treatment effect on the change in area of photoreceptor loss and a significant correlation between those two outcome measures.[10] Finally, it is possible that the observer response characteristics are different during a detection task where visual stimuli spans a wide range of intensities (and often near the visual threshold), compared to a detection task involving only suprathreshold stimuli; future studies are required to examine this. Anecdotally, most participants reported that the defect-mapping strategy being easier to perform, and there were, indeed, more unreliable tests recorded when using the thresholding strategy.

The relative effectiveness of the defect-mapping approach would be dependent on the nature of visual function abnormalities in different retinal diseases. The use of the ONH of healthy individuals provided a model of a deep and localized scotoma, where there is a marked difference in sensitivities within and outside the ONH. This model would seem representative of eyes with atrophic AMD, given recent observations that microperimetric visual sensitivity thresholds immediately outside the border of atrophic regions were similar to the more distal non-atrophic regions,[25,26] indicating how visual sensitivity losses are often deep and localized within atrophic regions. A similar observation of a marked difference in visual sensitivity within areas of photoreceptor loss or retinal pigment epithelium degeneration and unaffected retinal regions also has been reported in eyes with IRDs.[15,27–29] However, it should be acknowledged that use of the ONH in young, healthy volunteers as a model of deep scotomas and simulation of its progressive enlargement through reducing the size of the stimulus pattern is only intended to provide a preliminary assessment of this approach. Future studies are needed to compare the effectiveness of the defect-mapping and thresholding strategies in actual eyes with atrophic AMD and IRDs, and also to understand which approach better reflects self-reported visual disability.

A limitation of this study is that the defect-mapping strategy used a single stimulus intensity (of 10 dB) when examining all test locations. However, a defect-mapping

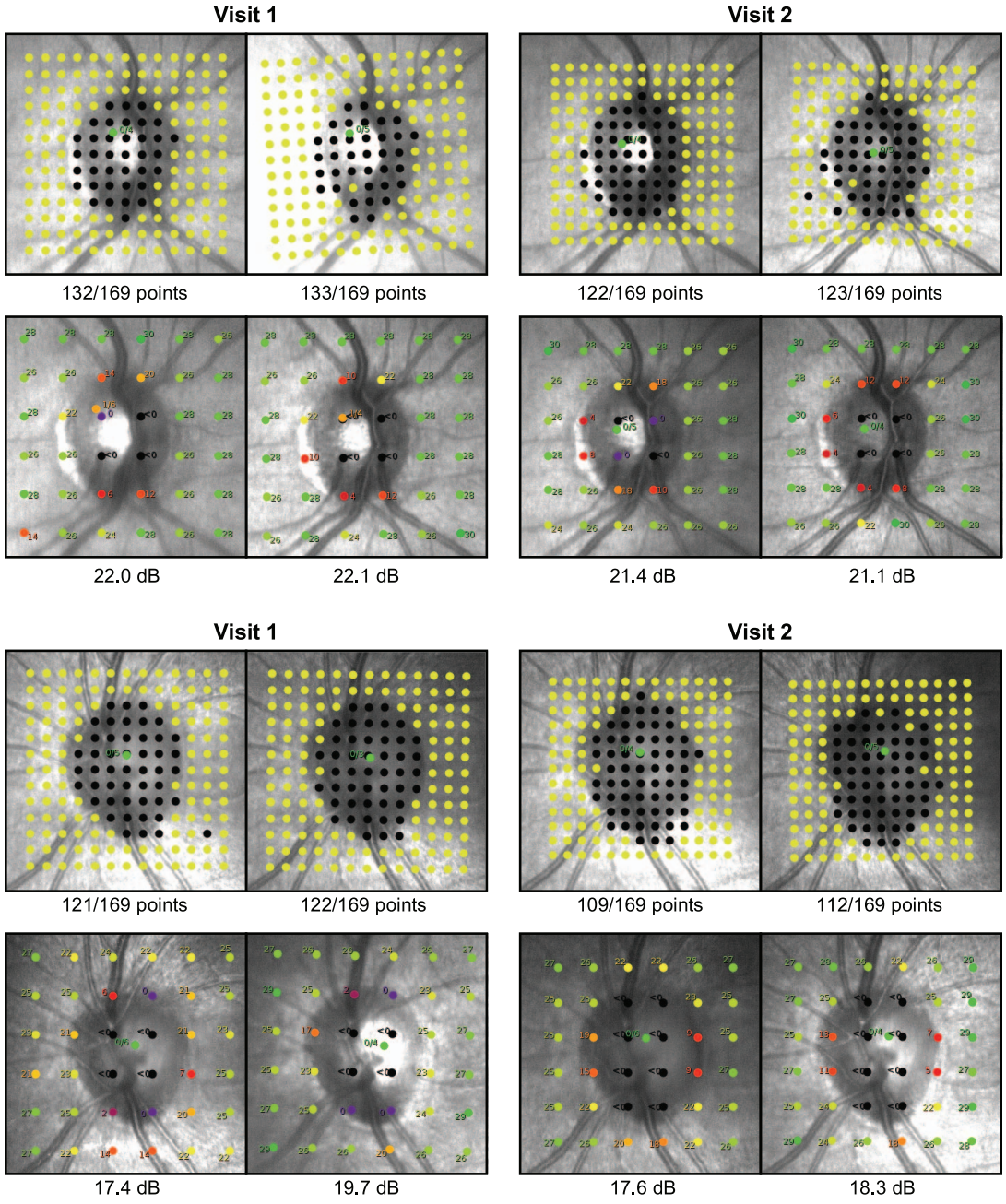

Figure 5. Examples of change over time simulated by decreasing the size of the stimulus pattern from the second compared to the first visit for the defect-mapping (top in each example) and threshold (bottom in each example) microperimetry testing strategies in this study from two different representative participants, with the outcome measures being the proportion of locations seen and mean sensitivity respectively. Note that the additional test location that is not consistent with the isotropic stimulus pattern represents the location where the false-positive catch trials were presented.

approach should ideally account for topographic variations in normal visual sensitivity, and this approach could be enabled by future software updates by the device manufacturers. The defect-mapping strategy also could be improved in future studies through the use of more efficient testing algorithms that avoids redundant retesting of established deep scotomas, but instead increases the sampling density at its borders.[30–32] Improved testing efficiency could also be achieved by incorporating structural information to guide the customized placement of test locations.[26,33–35]

In conclusion, this study demonstrated that a defect-mapping strategy on microperimetry testing enabled the progressive enlargement of deep scotomas

to be more effectively captured than the conventional thresholding strategy, with a nearly 2-fold improvement in the degree of change detected relative to measurement variability. These findings underscored the potential value of a defect-mapping microperimetry testing strategy as an effective outcome measure in clinical trials of atrophic AMD and IRDs and warrants further investigation in such eyes.

Acknowledgments

Supported in part by a National Health & Medical Research Council Principal Research Fellowship (GNT1103013, RHG) and Early Career Fellowship (#1104985, ZW). The Centre for Eye Research Australia receives operational infrastructure support from the Victorian Government.

Disclosure: **Z. Wu**, None; **R. Cimetta**, None; **E. Caruso**, None; **R.H. Guymer**, Bayer, Novartis, Roche Genentech, and Apellis (outside the submitted work; I), Bayer (outside the submitted work; F)

References

1. Csaky K, Ferris F, Chew EY, et al. Report From the NEI/FDA Endpoints Workshop on age-related macular degeneration and inherited retinal diseases. *Invest Ophthalmol Vis Sci*. 2017;58:3456–3463.
2. Wong WT, Kam W, Cunningham D, et al. Treatment of geographic atrophy by the topical administration of OT-551: results of a phase II clinical trial. *Invest Ophthalmol Vis Sci*. 2010;51:6131–6139.
3. Wong WT, Dresner S, Forooghian F, et al. Treatment of geographic atrophy with subconjunctival sirolimus: results of a phase I/II clinical trial. *Invest Ophthalmol Vis Sci*. 2013;54:2941–2950.
4. MacLaren RE, Groppe M, Barnard AR, et al. Retinal gene therapy in patients with choroideremia: initial findings from a phase 1/2 clinical trial. *The Lancet*. 2014;383:1129–1137.
5. Bainbridge JW, Mehat MS, Sundaram V, et al. Long-term effect of gene therapy on Leber's congenital amaurosis. *N Engl J Med*. 2015;372:1887–1897.
6. Chew EY, Clemons TE, Peto T, et al. Ciliary neurotrophic factor for macular telangiectasia type 2: results from a phase 1 safety trial. *Am J Ophthalmol*. 2015;159:659–666. e1.
7. Park SS, Bauer G, Abedi M, et al. Intravitreal autologous bone marrow CD34+ cell therapy for ischemic and degenerative retinal disorders: preliminary phase 1 clinical trial findings. *Invest Ophthalmol Vis Sci*. 2015;56:81–89.
8. Petrou PA, Cunningham D, Shimel K, et al. Intravitreal sirolimus for the treatment of geographic atrophy: results of a phase I/II clinical trial. *Invest Ophthalmol Vis Sci*. 2015;56:330–338.
9. Wagner SK, Jolly JK, Pefkianaki M, et al. Transcorneal electrical stimulation for the treatment of retinitis pigmentosa: results from the TESOLAUK trial. *BMJ Open Ophthalmology*. 2017;2.
10. Chew EY, Clemons TE, Jaffe GJ, et al. Effect of ciliary neurotrophic factor on retinal neurodegeneration in patients with macular telangiectasia type 2: a randomized clinical trial. *Ophthalmology*. 2019;146:540–549.
11. Cukras C, Wiley HE, Jeffrey BG, et al. Retinal AAV8-RS1 gene therapy for X-linked retinoschisis: initial findings from a phase I/IIa trial by intravitreal delivery. *Mol Ther*. 2018;26:2282–2294.
12. Dimopoulos IS, Hoang SC, Radziwon A, et al. Two-year results after AAV2-mediated gene therapy for choroideremia: the Alberta experience. *Am J Ophthalmol*. 2018;193:130–142.
13. Lam BL, Davis JL, Gregori NZ, et al. Choroideremia Gene therapy phase 2 clinical trial: 24-month results. *Am J Ophthalmol*. 2019;197:65–73.
14. Le Meur G, Lebranchu P, Billaud F, et al. Safety and long-term efficacy of AAV4 gene therapy in patients with RPE65 Leber congenital amaurosis. *Mol Ther*. 2018;26:256–268.
15. Cideciyan AV, Swider M, Aleman TS, et al. Macular function in macular degenerations: repeatability of microperimetry as a potential outcome measure for ABCA4-associated retinopathy trials. *Invest Ophthalmol Vis Sci*. 2012;53:841–852.
16. Testa F, Melillo P, Di Iorio V, et al. Macular Function and morphologic features in juvenile Stargardt disease: longitudinal study. *Ophthalmology*. 2014;121:2399–2405.
17. Jolly JK, Xue K, Edwards TL, et al. Characterizing the natural history of visual function in choroideremia using microperimetry and multimodal retinal imaging. *Invest Ophthalmol Vis Sci*. 2017;58:5575–5583.
18. Schönbach EM, Wolfson Y, Strauss RW, et al. Macular sensitivity measured with microperim-

etry in Stargardt disease in the Progression of Atrophy Secondary to Stargardt Disease (ProgStar) Study: report No. 7. *JAMA Ophthalmology*. 2017;135:696–703.
19. Iftikhar M, Kherani S, Kaur R, et al. Progression of retinitis pigmentosa as measured on microperimetry: the PREP-1 Study. *Ophthalmology Retina*. 2018;2:502–507.
20. Wu Z, Jung CJ, Ayton LN, et al. Test–retest repeatability of microperimetry at the border of deep scotomas. *Invest Ophthalmol Vis Sci*. 2015; 56:2606–2611.
21. Wu Z, Ayton LN, Guymer RH, Luu CD. Intrasession test–retest variability of microperimetry in age-related macular degeneration. *Invest Ophthalmol Vis Sci*. 2013;54:7378–7385.
22. Gardiner SK, Fortune B, Demirel S. Signal-to-noise ratios for structural and functional tests in glaucoma. *Trans Vis Sci Tech*. 2013;2:3.
23. Wu Z, Weng DSD, Thenappan A, et al. Evaluation of a region-of-interest approach for detecting progressive glaucomatous macular damage on optical coherence tomography. *Trans Vis Sci Tech*. 2018;7:14.
24. Wu Z, Thenappan A, Weng DSD, et al. Detecting glaucomatous progression with a region-of-interest approach on optical coherence tomography: a signal-to-noise evaluation. *Trans Vis Sci Tech*. 2018;7:19.
25. Hariri AH, Tepelus TC, Akil H, et al. Retinal sensitivity at the junctional zone of eyes with geographic atrophy due to age-related macular degeneration. *Am J Ophthalmol*. 2016;168:122–128.
26. Pfau M, Müller PL, von der Emde L, et al. Mesopic and dark-adapted two-color fundus-controlled perimetry in geographic atrophy secondary to age-related macular degeneration (published online ahead of print October 8, 2018). *Retina*.
27. Edwards TL, Groppe M, Jolly JK, et al. Correlation of retinal structure and function in choroideremia carriers. *Ophthalmology*. 2015;122: 1274–1276.
28. Asahina Y, Kitano M, Hashimoto Y, et al. The structure-function relationship measured with optical coherence tomography and a microperimeter with auto-tracking: the MP-3, in patients with retinitis pigmentosa. *Sci Rep*. 2017;7:15766.
29. Sallo FB, Leung I, Clemons TE, et al. Correlation of structural and functional outcome measures in a phase one trial of ciliary neurotrophic factor in type 2 idiopathic macular telangiectasia. *Retina*. 2018;38:S27–S32.
30. Chong LX, McKendrick AM, Ganeshrao SB, Turpin A. Customized, automated stimulus location choice for assessment of visual field defects. *Invest Ophthalmol Vis Sci*. 2014;55:3265–3274.
31. Chong LX, Turpin A, McKendrick AM. Targeted spatial sampling using GOANNA improves detection of visual field progression. *Ophthalmic Physiol Opt*. 2015;35:155–169.
32. Chong LX, Turpin A, McKendrick AM. Assessing the GOANNA visual field algorithm using artificial scotoma generation on human observers. *Trans Vis Sci Tech*. 2016;5:1.
33. Ganeshrao SB, McKendrick AM, Denniss J, Turpin A. A perimetric test procedure that uses structural information. *Optom Vis Sci*. 2015;92: 70–82.
34. Ganeshrao SB, Turpin A, McKendrick AM. Sampling the visual field based on individual retinal nerve fiber layer thickness profile. *Invest Ophthalmol Vis Sci*. 2018;59:1066–1074.
35. Alluwimi MS, Swanson WH, Malinovsky VE, King BJ. Customizing perimetric locations based on en face images of retinal nerve fiber bundles with glaucomatous damage. *Trans Vis Sci Tech*. 2018;7:5.